In silico modelling of long bone healing involving osteoconduction and mechanical stimulation

Jean-Louis Milan, Ian Manifacier, Nicolas Rousseau, Martine Pithioux

In silico modelling of long bone healing involving osteoconduction and mechanical stimulation.

Jean-Louis Milan [a,b,c,d], Ian Manifacier [a,b,c,d], Nicolas Rousseau [a,b,c,d,e], Martine Pithioux [a,b,c,d]

[a] Aix Marseille Univ, CNRS, ISM, Marseille, France;
[b] Aix Marseille University, Marseille Public University Hospital System (APHM), French National Center for Scientific Research (CNRS), Institute of Movement Science (ISM), Sainte Marguerite Hospital, IML, Department of Orthopedics and Traumatology Marseille, France;
[c] Aix Marseille University, Marseille Public University Hospital System (APHM), French National Center for Scientific Research (CNRS), Anatomic laboratory, Timone, Marseille, France;
[d] Aix Marseille University, Mecabio Platform, French National Center for Scientific Research (CNRS), Marseille, France
[e] Selenium Medical, La Rochelle, France

Abstract

Large diaphyseal fractures is one of most challenging fractures to treat. More research is needed to reliably promote diaphyseal bone healing. Many research projects currently aim to understand and guide the long bone repair and consolidation. These projects typically involve in vivo or in vitro models. Moreover, new osteoconductive and osteoinductive biomaterials are developed to promote bone formation. In addition, a lot of evidence has shown the importance of stimulating cell mechanically during bone repair. However, the mechanical environment proposed to cells within a porous biomaterial is difficult to evaluate. More importantly, after a bone fracture, there is no precise management of mechanical stimulation during a patient's rehabilitation that involves an adapted therapy program guided by modern measuring tools. Instead, we believe that theoretical and numerical mechanobiological models of bone repair could become practical tools to narrow down key parameters before moving to in vivo experiments. It then seems logical that modeling can be useful to optimize mechanical stimulation during a patient's rehabilitation. In this study, we modeled the fracture healing of a large bone defect in tibial diaphysis. To fill the fracture gap, we considered the implantation of a porous osteoconductive biomaterial made of poly-lactic acid wrapped by a hydrogel membrane mimicking osteogenic properties of the periosteum. We identified the optimal loading case that best promotes the formation and differentiation into bone tissue within the diaphyseal bone defect. Our results support the idea that a patient's rehabilitation program should be adapted to reproduce optimal mechanical stimulations.

1. Introduction

In many instances natural bone healing and consolidation leads to the complete reconstruction of the injured tissue. The periosteum, a highly vascularized bone envelop, is a major contributor to the healing process. The periosteum acts as a clear boundary between the area where bone tissue must regrow and surrounding tissues. In addition, the periosteum favors the supply of mesenchymal cells that can differentiate into osteoblasts and synthesize bone matrix. Unfortunately, in the case of large bone lesions of either pathological (tumorous or infectious) or traumatic origin, the periosteum may be completely damaged. As a result, the risk of inadequate bone reconstruction remains significant and unpredictable. Such lesions may result in a pseudo arthrosis preventing any future consolidation [Rolland1995].

Moreover, the success of bone consolidation may depend on location. Epiphyseal and metaphyseal fractures consolidate more rapidly than diaphyseal ones. The great majority of diaphyseal fractures are secondary to trauma, which can be associated to cutaneous and vascular lesions. The most frequent diaphyseal lesion in healthy humans is the fracture of the tibia. The loss of diaphyseal osseous tissue is a difficult problem in traumatology due to soft tissues lesions that in turn lead to a significantly higher risks of infection [Masquelet2012].

Bone fracture healing is influenced by many factors and mechanics is an important one [Victoria2010]. Proper consolidation cannot occur without immobilization. However, strict immobilization is neither essential nor optimal. Instead, limited mobility enables mechanical strain and fluid flow induced shear stresses, both of which contributes to the proper development of a bone callus. However, excessive mobility leads to high fluid induced shear stresses that are in turn detrimental to consolidation [Palomares2010].

To stabilize the fracture gap, the surgeon uses osteosynthesis plates and external fixators. External fixators have the advantage of not interfering with the site of injury while shielding the fracture gap from excessive external mechanical forces. Nonetheless external fixators increase the risk of delayed consolidation. Serious infection can occur on pin paths and may lead to death a few years later. Therefore, amputations by primary intention or in case of functional failure remains a surgical solution [Masquelet2012]. Fracture healing failures highlight a poor understanding of the whole process and in particular the role of the periosteum. Indeed, on this last point, we have previously demonstrated in animal models that a well-preserved and well-vascularized periosteum can induce the complete regeneration of a large bone gap after 3 weeks [Casanova2010].

Although, it is necessary to limit the relative mobility between the proximal and distal tibial fragments, associated joint stiffening and muscular atrophies must also be avoided. Support must be

progressive from complete discharge to full weight loading. In the case of diaphyseal leg fractures, external fixators have the advantage of allowing patient to walk sooner. The present study analyzed the potential of scalable external fixators that could allow limited and controlled interfragmentary movement (IFM). Such a system is not yet widely used in orthopedics. Nevertheless, it could mechanically stimulate the bone callus and accelerate fracture healing.

In orthopedic surgery, the use of biomaterial meant to bear the mechanical load during the recovery process is expanding. Many research projects focalize on the improvement of the osteoconductive and osteoinductive properties of biomaterials and their ability to properly recruit osteopotent stem cells from bone marrow. For instance, Navarro et al. in 2006 developed a porous biodegradable material composite made of poly lactic acid (PLA). Its mechanical properties closely matched those of bone tissue and promote bone tissue formation [Navarro2006]. Harris et al. 2008 studied in vitro cell proliferation and differentiation within this bioactive ceramic [Harris2006]. Furthermore, biomaterials made of resorbable hydrogels are good candidates for tissue engineering [Yue2020]. They have properties similar to the native extracellular matrix and thus promote cell adhesion and proliferation. Hydrogel membranes were developed to perform the function of biological membranes promoting hemostasis and bone regeneration. These membranes consisted of porcine collagen, polycaprolactone, or polyethylene glycol [Wang2016]. Hydrogel membranes could be used to replicate the crucial role of the periosteum in the healing process of large bone defects [Coïc2010; Oliveira2010; Sheikh2015].

To quantify and predict the influence of mechanical stimulation on bone fracture healing, numerical approaches were developed. One of the most widely used is that based on mechanoregulation theory which predicts cell differentiation and tissue formation as a function of the range of fluid and solid mechanical stimuli [Prendergast1997; Lacroix2002). We used this approach to model bone tissue formation in a porous biomaterial [Milan2010]. Checa et al. in 2010 also used a numerical model to study tissue differentiation and repair of a diaphyseal fracture [Checa2010]. On the same note, Sandino et al. 2010 analyzed the formation of bone within a phosphor-calcium biomaterial by simulating angiogenesis [Sandino2010].

In line with previous work, we propose here a in silico model of tibial bone healing. More precisely, this model applies to a large diaphyseal defect. With the model, we analyzed the benefits of implanting an osteoconductive biomaterial in conjunction with a mechanically oriented rehabilitation program. The biomaterial was shaped as a hollow cylinder made of porous PLA wrapped in a hydrogel membrane. Tissue formation was predicted by the mechanoregulation algorithm. As a result, we define the optimal mechanical stimulation to promote bone defect healing. Our results provide

additional knowledge to optimize therapeutic management in orthopedics and enable faster and more complete functional recovery.

2. Methods

Bone formation and tissue differentiation were simulated according to a mechanoregulation algorithm. The latter is used to predict tissue phenotypes and their mechanical properties depending on local mechanical stimuli, which resulted from imposed mechanical loading on the tibia. We used a finite element method to calculate these stimuli.

2.1 Finite element model of damaged tibia

A frozen cadaveric tibia specimen from an 85-year old female was obtained from our Department of Anatomy at the Aix-Marseille University. The specimen was scanned using a standardized CT scan protocol led by CERIMED, Marseille, France using Discovery 710 device from GE Medical Systems with the following acquisition parameters: 120 kV, 400 mA and 0.625-mm-thick slices. DICOM images were imported into Mimics software (Materialise®, Leuven, Belgium) to numerically reconstruct the tibia in 3D and create, based on bone mass densities, a finite element model (Figure 1). To reproduce the gap of a long bone fracture, a diaphyseal bone deficit of 6 cm in length was created in the 3D reconstruction of the tibial bone. The proximal and distal part of the tibia is composed of 150,000 linear tetrahedra (type C3D4). The quality of the tibia and biomaterial meshes was validated by Abaqus mesh verification analysis, keeping the standard threshold values proposed by default and following the recommendations of Burkhart et al. 2013 [Burkhart2013] (Table 1).

a

b

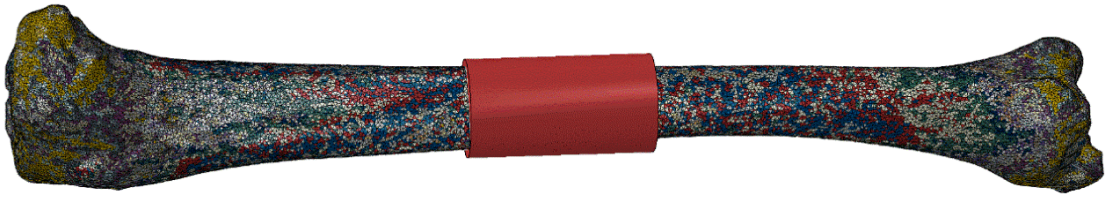

Figure 1*: Finite element model of the tibia with a biomaterial colored in red implanted in a large diaphyseal lesion. Views of the model in the front (a) and the sagittal (b) plane.*

Meshed Part	Tibia	Biomaterial
Number of elements	152 076	4 320
Shape of elements	Tetrahedral	Hexahedral
Type	Linear	Linear
Percentage of elements with Min angle on Triangle Faces < 5°	0%	0%
Average Min face corner angle	28.57°	84.61°
Worst Min face corner angle	6.61°	82.39°
Percentage of elements with Max face corner angle < 170°	100%	100%
Percentage of elements with Max face corner angle < 120°	**96.28%**	**100%**
Average Max face corner angle	98.80°	95.43°
Worst Max face corner angle	163.33°	97.47°
Percentage of elements with Aspect ratio < 10	100%	100%
Average aspect ratio	2.22	1.39
Worst aspect ratio	7.89	1.85
Percentage of elements with Shape factor > 0.0001	100%	n/a
Percentage of elements with Shape factor > 3	**90.65%**	**n/a**
Average shape factor	0.43	n/a
Worst shape factor	2.38e-04	n/a
Percentage of elements with Stable time increment > 0.0001	100%	n/a
Average stable time increment	0.0076	n/a
Smallest stable time increment	4.61e-04	n/a
Percentage of elements with Min edge length > 0.01mm	100%	100%
Average min edge length (mm)	1.44	1.74
Shortest edge (mm)	0.12	1.18
Percentage of elements with Max edge length > 1mm	99.67%	100%
Average max edge length (mm)	2.99	2.37
Longest edge (mm)	23.47	3.01
Percentage of elements with Analysis errors	0%	0%
Percentage of elements with Analysis warnings	1.40 %	0%

Table 1 *- Mesh quality analysis for the tibia and the biomaterial. In red are the checks of mesh quality following the recommendations of Burkhart et al. 2013 [Burkhart2013].*

Each finite element of the tibial bone was defined as isotropic. However local linear elastic material properties were based on tomography Hounsfield units (HU). HU allowed us to derive local bone mass densities (ρ), which in turn allowed us to calculate the corresponding Young's moduli (E). We used 2 different sets of laws dedicated respectively to the tibia, one for the cortical (eq. 1, [Snyder1991]):

$$\begin{cases} \rho = 1 * HU, \ \ \rho \ in \ kg/m^3 \\ E = 0.06456 * \ \rho^{0.74}, \ \ E \ in \ GPa \end{cases} \quad \text{Eq. 1}$$

the other for the trabeculae [Hobatho1997]:

$$\begin{cases} \rho = 0.916 * HU + 114, \ \ \rho \ in \ kg/m^3 \\ E = 0.51 * \ \rho^{1.37}, \ \ E \ in \ GPa \end{cases} \quad \text{Eq. 2}$$

Poisson coefficient of tibia bone materials was set to 0.3.

To treat the bone gap defect, we considered a composite biomaterial made of a PLA scaffold in the shaped of a hollow cylinder and a hydrogel membrane wrapped around it. The PLA hollow cylinder was 60 mm in length with an external diameter of 25mm, a center hole diameter of 15 mm and a thickness of 5 mm. The PLA hollow cylinder approximated the diaphyseal hollow shape. The finite element model of the PLA scaffold was made of 6,500 linear C3D8R hexahedra. The hydrogel membrane was 60 mm in length and 5mm thick and was composed by 36,000 linear C3D8R hexahedra.

We considered that, after implantation, the PLA scaffold and hydrogel membrane became filled with biological fluids. They were represented by poroelastic materials whose properties are reported in Table 2.

	PLA scaffold	**Hydrogel membrane**
Young's modulus (kPa)	100	1
Poisson's coefficient	0.3	0.3
Permeability (m^4/Ns)	2 e^{-7}	1 e^{-10}
Porosity	0.95	0.8
Solid bulk modulus (MPa)	500	2300
Fluid bulk modulus (MPa)	2300	2300

Table 2*. Material properties of the PLA scaffold [Navarro2006; Charles-Harris2008] and the hydrogel membrane [Hwang2010].*

2.2 Loading and boundary conditions

We simulated a rehabilitation program in which the distal part of the tibia is compressed, cyclically every 1s and during 1-2 hours per day. We express each loading condition by the amplitude of compressive distal displacement which was applied per second (mm/s) and induced IFM in the diaphyseal bone defect. We tested 4 compressive rates: 0.3, 0.6, 1.8 and 3 mm/s. Then the mechanoregulation algorithm predicted the local tissue phenotype that would form within the PLA scaffold and hydrogel membrane after a 2-month long rehabilitation program. To obtain stable in silico predictions of tissue phenotypes and to reach convergence, the mechanoregulation algorithm was performed iteratively for every loading case. The media of the PLA scaffold and the hydrogel membrane were permeable with zero pressure at their boundaries except on the outer side of the membrane. A zero-velocity boundary condition was applied to the outer side the hydrogel membrane to simulate its impermeability that prevents cell invasion by surrounding soft tissue.

2.3 Mechanical Regulation Model

The diaphyseal lesion causes an influx of undifferentiated mesenchymal cells that colonize the porous biomaterial. It is essential that stem cells fully colonize the biomaterial. Otherwise, osteosynthesis may be compromised. However, in this study, our intention was only to consider the influence of mechanical stimulation on bone formation, we therefore assumed that the biomaterials were completely colonized by stem cells at the beginning of the simulation. Thus, during the simulation and throughout the porous biomaterial, stem cells were able to differentiate into fibroblasts, chondrocytes or osteoblasts according to the mechanoregulation algorithm shown in Figure 2. No other cell differentiation factor was considered. The procedure was iterated several times to achieve, when possible, convergence of the tissue phenotype due to mechanical stimulation. For each iteration, the mechanical stimulus ***S*** in each element of the PLA scaffold and hydrogel membrane was used to identify the phenotype of the new tissue and to update the properties of the materials. For each iteration, finite element analysis was performed under the same boundary and initial conditions via the Standard Abaqus solver (Dassault Systems Simulia Corporation).

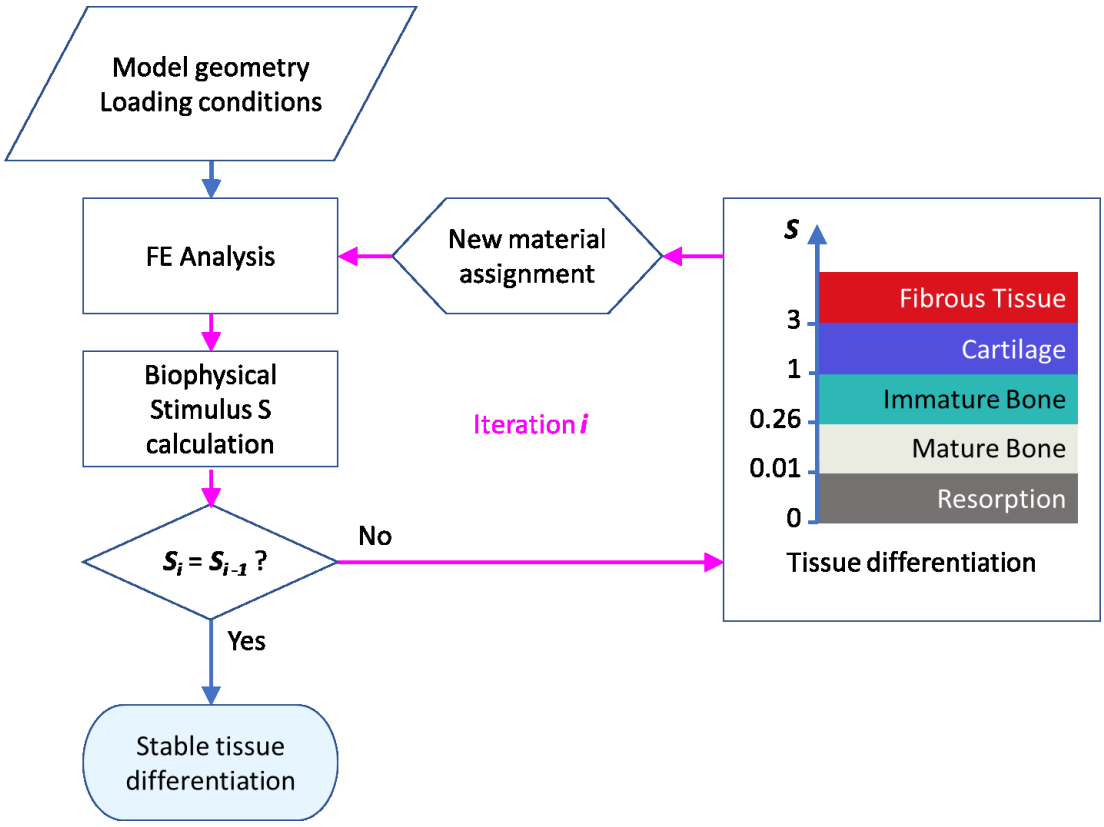

Figure 2*: Mechanoregulation algorithm. Iterative procedure and diagram of tissue differentiation following mechanical stimulus thresholds [Prendergast1997; Lacroix2002].*

The differentiation process was governed by the biophysical stimulus $\boldsymbol{S}$ as a combination of the shear strain $\boldsymbol{\varepsilon}$ in the tissue and the interstitial fluid velocity $\boldsymbol{v}$ (Eq. 3) [Prendergast1997; Lacroix2002],

$$\boldsymbol{S} = \boldsymbol{\varepsilon} / \boldsymbol{a} + \boldsymbol{v} / \boldsymbol{b} \qquad \text{(Equation 3)}$$

wherein $\boldsymbol{a}$ and $\boldsymbol{b}$ are equal to 3.75% and 3mm.s^{-1} respectively

As shown in in Table 3, we considered 4 different $\boldsymbol{S}$ thresholds to determine whether if the cells differentiate into fibroblasts, chondrocytes or osteoblasts, respectively leading to the formation of fibrous tissue, cartilage tissue or bone tissue. If cells were under stimulated ($\boldsymbol{S}$ <0.01067), the tissue was replaced by its granular counterpart.

No predetermined pathways led to tissue differentiation from one phenotype to another. The phenotype of the tissues at the iteration *i* did not depend on the phenotype at the iteration *i*-1 but only on $\boldsymbol{S}$ (*i*). The tissues were considered as poroelastic materials whose properties are given in Table 3. During the simulation, when tissue either formed inside the scaffold and the membrane, the corresponding elements were viewed as homogenized composites made of biological tissue and PLA or hydrogel. Since, the time required to degrade the biomaterial is much longer than the 2-month duration of the rehabilitation program, we assumed that the implant did not degrade and that its material properties remained unchanged [Navarro2006]. At the beginning of the simulation, all tissue contained within the pores of the biomaterial started as granular. We assumed that the mechanical properties of the liquid phase in the biological material remained unchanged during the simulation.

Tissue differentiation and formation correspond to a gradual process spanning over the rehabilitation period. However, the computation predicted only the final tissue phenotypes after 2 months of a daily stimulation rehabilitation program. Thus, an iteration of the algorithm did not correspond to a day of stimulation. Instead, it was a prediction of the final tissue phenotype after 2 months of stimulation based on the last differentiation factor $\boldsymbol{S}$ to be calculated. As a result, an iteration should be interpreted as an optimization step necessary to converge towards a stable solution. We consequently ran each simulation with enough iteration to observe convergence.

In this study, we analyzed the effect of dynamic compression cycles, distal displacement being imposed for a time of 1s with various compressive amplitudes. The overall procedure which included both mechanical computations and the mechanoregulation algorithm (Figure 2) was iterated 50 times. If the phenotype remained constant in 95% of biomaterial elements we consequently assumed that the simulation had converged.

	Granulation tissue	Mature bone	Immature bone	Cartilage	Fibrous tissue
Biophysical stimulus	$S < 0.01067$	$0.01067 < S < 0.267$	$0.267 < S < 1$	$1 < S < 3$	$S < 3$
Young's modulus (MPa)	0.2	6000	1000	10	2
Poisson's coefficient	0,167	0,3	0,3	0,167	0,167
Permeability (m^4/Ns)	$1\ e^{-14}$	$3,7\ e^{-13}$	$1\ e^{-13}$	$5\ e^{-15}$	$1\ e^{-14}$
Porosity	0,8	0,8	0,8	0,8	0,8
Solid bulk modulus (MPa)	2300	13920	13920	3400	2300
Fluid bulk modulus (MPa)	2300	2300	2300	2300	2300

Table 3*. Poroelastic properties of the specific tissue phenotypes promoted by biophysical stimuli, S [Lacroix2002; Checa2010]*

3. Results

The 3D finite element model of tibial bone with a diaphyseal bone deficit of 6 cm in length was obtained by image segmentation and the isotropic linear elastic material properties were assigned depending on local HU values (Figure 3).

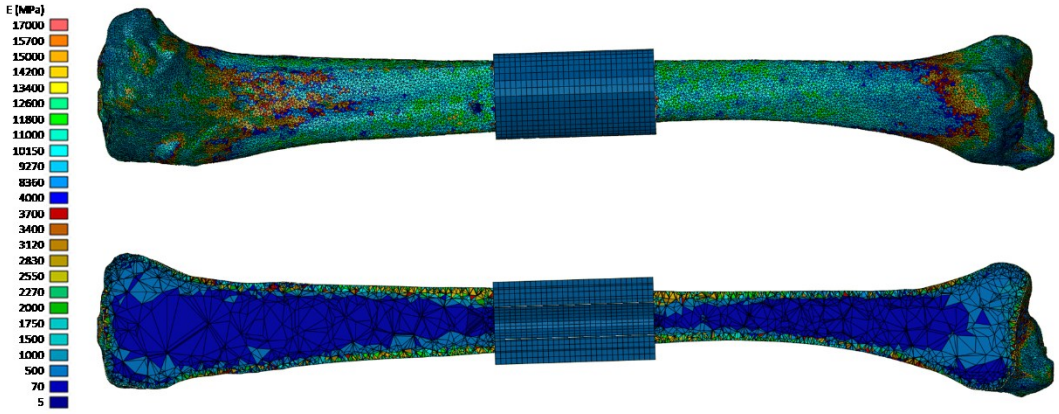

Figure 3*: Distribution of material properties expressed in terms of Young's modulus, E (MPa) in the finite element model of the tibia with the biomaterial implanted in the diaphyseal defect.*

After 50 optimization iterations, of the mechanoregulation algorithm, tissue had formed and differentiated within the implanted PLA scaffold and the hydrogel membrane (Figure 4). Results show that the final tissue phenotypes highly depend on the compressive rate applied on the tibial bone. In

the loading cases of 0.5mm/s and above, the distributions of tissue phenotypes are heterogenous in the diaphyseal direction. The distributions of tissue phenotype are quite homogeneous in the radial direction without any great variation between PLA scaffold and hydrogel membrane.

Figure 5 shows the proportions of final tissue phenotypes within the biomaterial. The results indicate an optimal stimulation scenario promoting the regeneration of mature bone tissue within the composite biomaterial. The loading condition of 0.1mm/s allowed up to 97% regeneration in mature bone. For lower rates of compression, cell apoptosis and tissue resorption were predicted due to insufficient mechanical stimulation. For higher compressive amplitudes, stable differentiation into mature bone tissue was not guaranteed, instead the model predicted the formation of cartilage and fibrous tissue. The increase in distal displacement, and consequently in IFM, induces large formation of cartilage up to 60% (Figure 5). At this point, by reducing distal displacement to 0.1 mm/s in the following loading cycles, we observed that the large amounts of cartilage then differentiated into mature bone, giving the same distribution of mature bone as that produced by imposing 0.1mm/s from start to finish.

Figure 6 shows the evolution of the proportion of mature bone for all loading cases during the iterative simulations. Figure 7 shows the evolution of the proportion of all tissue phenotypes during the optimal loading scenario of 0.1mm/s. In this scenario, maximal and stable formation of mature bone was predicted since the first iteration.

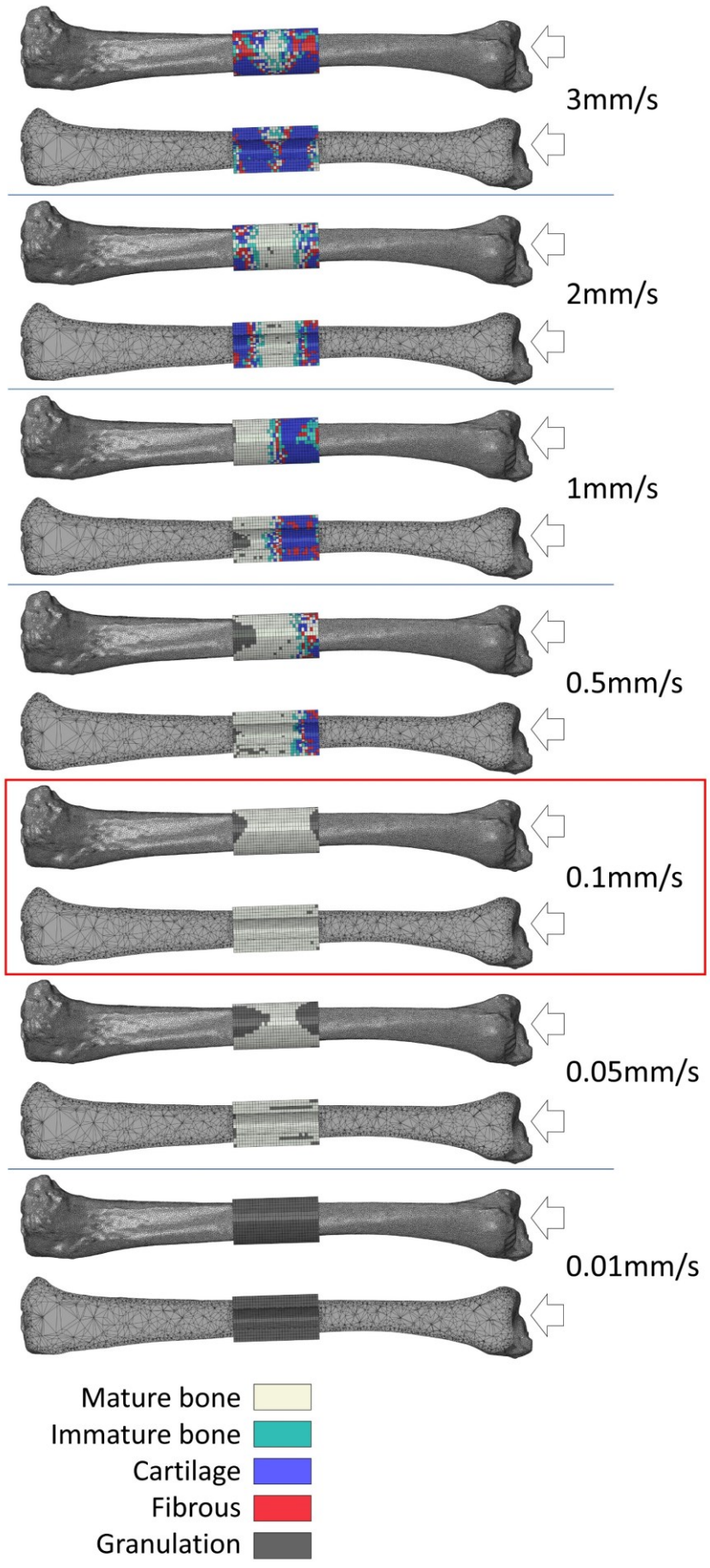

***Figure 4**: Distribution of tissue phenotypes formed within the PLA scaffold and the hydrogel membrane at the end of the simulation based on the loading scenario. For every loading case, the tibial bone and biomaterial are showed in the sagittal plane both in side-view and cut-view. Red box indicates the optimal condition of loading leading to mature bone differentiation.*

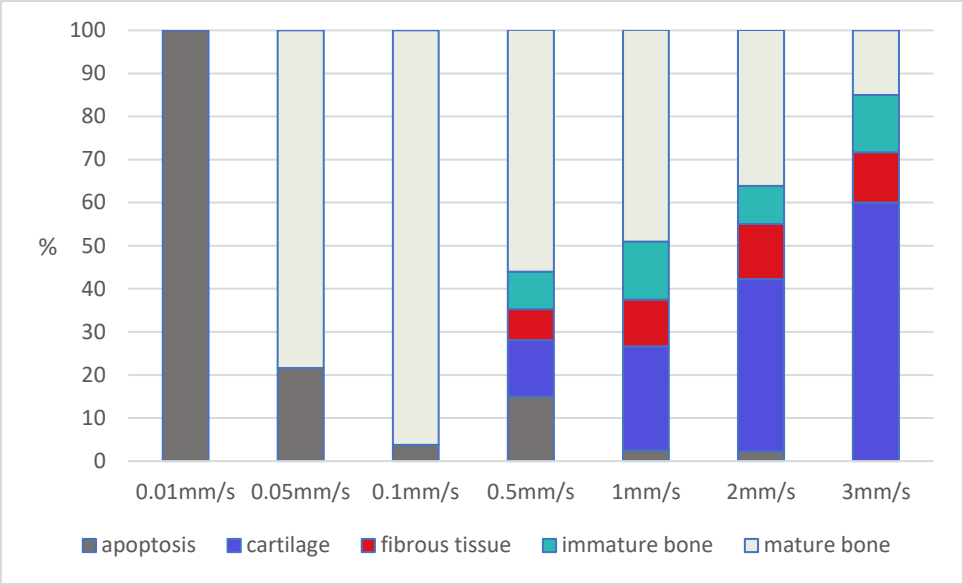

273

274 ***Figure 5**: Final percentage of each type of tissue formed in the PLA scaffold and hydrogel membrane*
275 *based on mechanical loading conditions.*

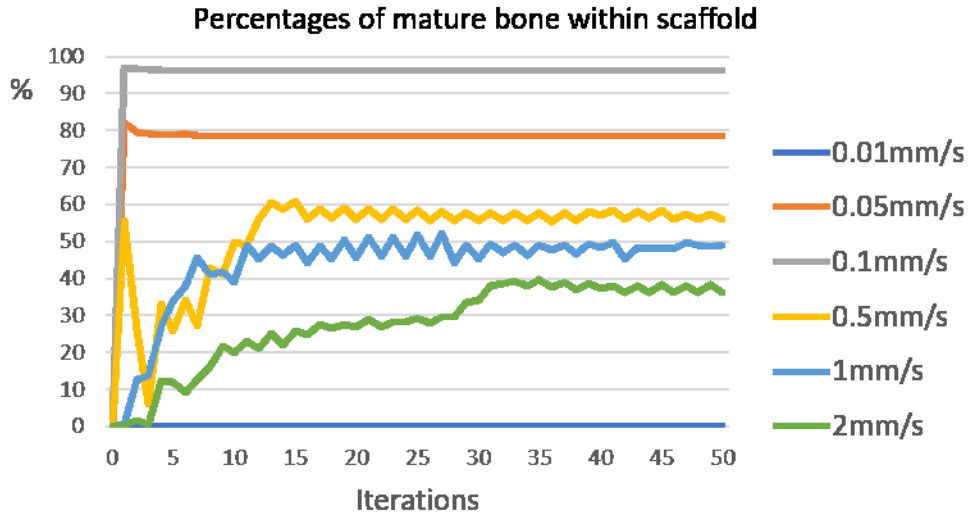

276

277 ***Figure 6**: Percentage of mature bone formed in the PLA scaffold and hydrogel membrane depending*
278 *on the iteration of tissue differentiation simulation for all loading cases.*

279

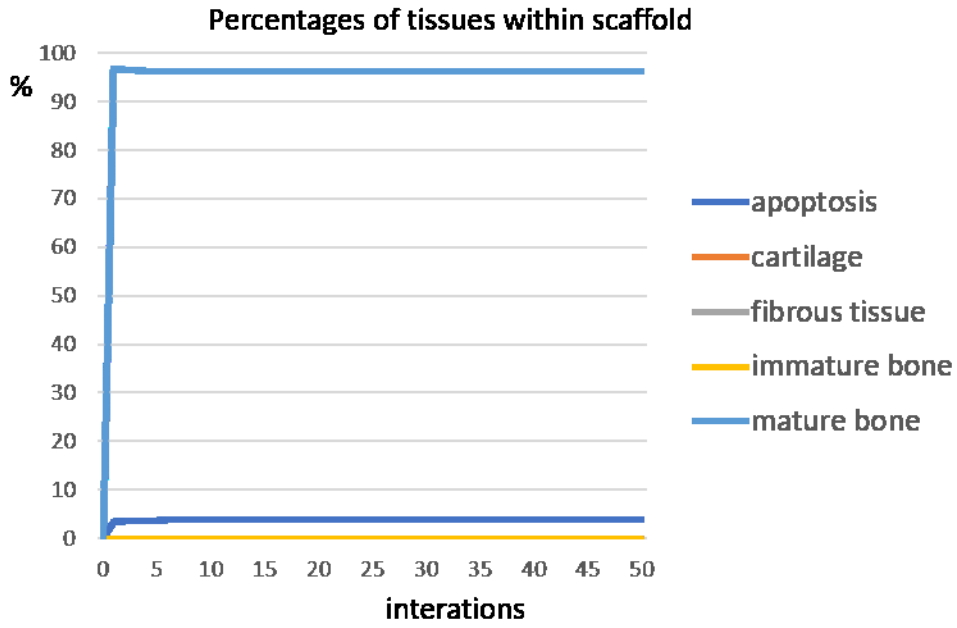

***Figure 7**: Percentage of tissues formed in PLA scaffold and hydrogel membrane depending on the iteration of tissue differentiation simulation for the loading case of 0.1 mm/s.*

4. Discussion

The objective of this study is to find the appropriate mechanical loading to promote bone healing of large tibial diaphyseal defect filled by a porous biomaterial. The biomaterial acting as a scaffold for tissue growth, we used the model of mechanoregulation to predict the effect of mechanical stimulation on the phenotype of the tissue that could form within the biomaterial.

4.1 Biomaterial design

The biomaterial was a hollow cylinder composed of a PLA scaffold wrapped with a hydrogel membrane. The hollow design is inspired by the geometry of the diaphysis. The hollow design allows for internal blood flow, bone marrow penetration and internal stem cell colonization. On the other hand, the hydrogel membrane that surrounds it, promotes the regeneration of the periosteum providing local vascularization and recruitment of stem cells, which are essential for bone healing. The semi-permeable hydrogel membrane protects the bone defect from invasion by peripheral soft tissue.

Casanova et al. 2010 have shown, *in vivo*, that the periosteum alone can regenerate a large bone volume. In the case of a major trauma, it is therefore necessary to find a biomaterial that serves as an

299 envelope and allows the regeneration of the periosteum. The hollow cylinder made of PLA foam acts
300 as a scaffold and the collagen membrane will allow regeneration of the periosteum.

301 **4.2 Mechanoregulation model prediction**

302 To stimulate bone healing mechanically, it is necessary to precisely know the required mechanical
303 conditions for bone regeneration. This consequently involves stem cells differentiating into active
304 osteoblasts. The numerical model of mechanoregulation developed by Prendergast and Lacroix
305 simulates the mechanobiological effect on bone regeneration and is able to identify the optimal
306 loading scenario [Prendergast1997; Lacroix2002].

307 The model of mechanoregulation was validated on several clinical applications such as fracture
308 repair, mandibular bone distraction and several in vitro experiments of bone formation in porous
309 biomaterials [Isaksson2006; Boccaccio2008; Checa2010; Milan2010; Sandino2010]. We therefore used
310 this model to determine the influence of mechanical stimulation on bone regeneration in a large
311 diaphyseal defect.

312 After the first optimization step of the mechanoregulation algorithm, we may already have some
313 indication of the expected outcome. However, in some instances the proportion attributed to each
314 tissue phenotype fluctuates slightly between iterations.

315 The relevance of the prediction of the mechanoregulation algorithm relies primarily on the
316 stability of local tissue phenotypes. This stability results from the fact that the local solid strain and
317 fluid flow are within the stimuli domain that would lead to the same tissue phenotype.

318 This stability is not always achieved. Tissue differentiation is the result of a specific biophysical
319 stimulus $\boldsymbol{S}$ value, calculated at one iteration based on local strain and fluid flow. As a consequence,
320 tissue differentiation results due to the changes in local stiffness, porosity and permeability, which in
321 turn, may profoundly modify the value of biophysical stimulus $\boldsymbol{S}$ that will be calculated in the next
322 iteration. One of the challenges of this study is be to find a solution that maintains the already formed
323 mature bone, between iterations and also differentiates immature bone, cartilage and fibrous tissue
324 into mature bone. Compared with the other scenarios, the 0.1 mm/s scenario led to a rapid
325 convergence and a very stable mature bone distribution. Moreover, if we assume that convergence
326 was achieved when less than 5% of the regenerated tissue volume experienced phenotype
327 fluctuations, regardless of the predicted dominant phenotype, our results indicate that stability was
328 achieved for all mechanical stimulation scenarios.

329 **4.3 Imposing force or displacement on bone fracture callus?**

Mechanical stimulation of the bone should be included in the early phases of the healing process. In the case of the tibia this may be achieved by walking with crutches. Early weight-bearing is limited by the fixation device which provides most of the support, leaving a limited part of the load to be transmitted through the bone callus. Considering large long diaphyseal defects, the implantation of a scaffold and the application of mechanical loading allow bone tissue formation as observed in vivo in sheep by Pobloth et al. 2018 [Pobloth2018]. Diaphyseal defect was stabilized by a locking compressive plate. The mechanical stimulation was introduced by allowing the sheep to walk, the load applied to the scaffold being a portion of body weight. By implementing a mechanoregulation model, Perier-Metz et al. 2020 reproduced in silico the experimental conditions of Pobloth et al. 2018 and simulated the same results of bone healing [Perier-Metz2020]. Bone healing was the result of the mechanical loading of the tissue that grew within scaffold pores. Mechanical stimulus depended on the level of stabilization of locking plate and on the mechanical properties of the scaffold. However, it is hard to predict the mechanical environment of the growing tissue and the studies did not report the deformation and displacement that were generated globally and locally.

Most studies that analyzed mechanical stimulation of long bone healing did so through early loading, imposing a near-constant level of force on the fracture callus. In our opinion, this is where the problem lies. In fact, the growing tissue has mechanical properties that gradually evolve first from a very soft, non-differentiated and non-mineralized granulation tissue to a very rigid and mineralized mature bone. The tissue formed after a few days may be not able to withstand the same mechanical loading as a tissue that had 2 weeks to form without excessive deformation. Of course, mineralized mature bone does not appear immediately. It is the result of successive differentiations involving, in particular, the transformation of granulation tissue into a cartilaginous callus, which gradually calcifies. During the regeneration, the progressive stiffening of the callus induces a necessary decrease in strain amplitudes that in turn stimulate bone matrix synthesis. At first, early weight-bearing can lead to high strains stimulating the differentiation of stem cells into chondrocytes. Chondrocytes will synthesize cartilage, stiffer, capable of supporting the applied load and drastically reducing the strain level, thus promoting bone differentiation. However, producing local strain by imposing global force is very risky and can impair bone healing if local strain becomes too high. Since the level of local strain is what matters at the cellular level, it would be better to control the local and global strains rather than impose a global force. From our point of view, the complete and viable healing of a fracture or a bone defect requires strain stimulation. This is exactly what we propose in our study. We propose to impose limited distal displacements to better control local deformations. We believe that this approach may be more promising than the current force-dependent standard achieved by applying a fraction of the

patient's weight. Producing local strain by distal displacement is simple to monitor and is closer to what is needed to stimulate cells within growing tissue.

4.4 Level of interfragmentary strains

Perren postulated in 2015 that for interfragmentary strains that exceed 2%, fibrocartilage or granulation tissue can form but no direct bone formation can occur [Perren2015]. On the contrary, Claes et al. in 1997 observed in an in vivo sheep model that larger interfragmentary strains at the very beginning shortened healing time of long hind leg bones fractures [Claes1997]. They showed that an initial interfragmentary strain of up to 30% still allowed bone fractures to heal. For large gaps, fast bone healing occurred with lower strain (7%). In 1997, Gardner et al. reported that the same positive influence of early high interfragmentary strains can occur in patients during early weight bearing. These results were obtained via instrumented external fixator on patients with tibial shaft fractures [Gardner1997]. In the very early healing phase, interfragmentary strains, ranging between 30% and 100%, produced some stimulatory effects and did not obstruct the repair process. In 2017, Bartnikowski et al. observed faster bone healing under evolutive interfragmentary strains. Using a fixator with an adjustable stiffness, they introduced large deformations at the very beginning, then gradually reduced them as ossification occurred [Bartnikowski2017].

In a patient-specific case, Wehner et al. 2010 demonstrated bone healing of a large tibial fracture, approximately 2.5 times the diaphyseal diameter, using a flexible fixator and early loading [Wehner2010]. Experimentally, bone fracture healed and initial maximum IFM was 1.5mm. By using a mechanobiological model, the authors predicted faster bone healing with an optimal IFM of 0.5mm.

In accordance with the studies cites above, our present findings reiterate on the importance of the IFM. In our study, we found that, during the healing period, a distal displacement of 0.1 mm per 1s cycles led to complete and mature ossification of the diaphyseal defect. At the very beginning of the simulation, the biomaterial was very soft and the IFM was equal to 0.1mm per cycles with interfragmentary strain of 0.17%.

This level of stimulation is consistent with one we identified in a previous in silico study based on exactly the same mechanoregulation algorithm. At the time, we obtained mature bone formation within cylindrical PLA scaffold (height 10mm, diameter 6mm; porosity 95%; pore size ~100-500µm) under 0.5%-1% of compression applied in cycles of 2s [Milan2010]. This level of stimulation is consistent with the results we obtained via our previous in silico studies based on the same mechanoregulation algorithm. Zhao et al. 2018 reported that a strain of 0.5% induced bone formation within a soft porous scaffold (pore size 300µm; porosity 70%) made of hydrogel (E= 2.3GPa) [Zhao2018].

The literature indicates that large IFMs at the very beginning followed by a significant IFM reduction accelerate bone healing. In our present study, low IFMs ensure mature bone formation at the end, while higher IFM induces substantial cartilage formation, which can reach up to 60% of the overall tissue volume (Fig 4 & 5). We observed that the large amounts of cartilage that were produced by high IFM, then differentiated into mature bone if IFM was drastically reduced. The final distribution of mature bone was the same as that produced by a low IFM imposed from start to finish. Our results suggest that the positive consequence of a large early IFM is to promote the prior formation of cartilage as a transition tissue to mature bone, eventually accelerating bone healing.

4.5 Isotropic linear elastic material properties of the tibia bone

We developed a finite element model of the tibia. Local Young's modulus values were based on the mineral density values acquired by a tibia tomography. This led to a heterogeneous model that represented the local material properties throughout the whole tibia bone, this method was consequently more accurate than in a homogeneous model [Taddei2006]. We also considered the common assumption of representing bone tissue as an isotropic elastic material. However, the material properties of long bones have been characterized as anisotropic, while the cortical is considered transversely isotropic. Anisotropic power-law relationships have been identified to determine the component of Young's modulus in the axial and transverse directions, based on bone density [Wirtz2000, Taylor2002].

Some studies compared isotropic and anisotropic models of femur based on Hounsfield unit values and power law [Peng2006, Yang2010, Ün2016, Hamandi2022]. Peng et al. 2006 reported that isotropic and anisotropic femur models give very similar results in loading conditions simulating standing. Stress and nodal displacement differ by only 0.6% and 1.2% respectively. Hamandi et al. 2022 simulated gait loading on femur models and showed that the average and maximum stresses were only 1.80% and 3.9% higher, respectively, in the model with elastic properties compared with the anisotropic model [Hamandi2022]. By extrapolating these results to the tibia we can safely assume that an isotropic model is accurate enough. Ün et al. in 2016 showed that under axial compression, anisotropic and isotropic material models of tibia produced very similar von Mises stress distribution of over the length of the tibia [Ün2016]. Since material properties variations have a stronger effect on strain than on stress, Ün et al. noted that, under pure compression, the isotropic model overestimated the maximum von Mises strain in the middle of the diaphysis by 10% compared to the anisotropic model. However, the authors did not give the error on the axial diaphyseal strain which should be less than 10% and which is the one that impacts the biomaterial in our study. The authors concluded that

anisotropic properties should be preferred for studies focusing on local bone strength or damage accumulation.

Considering the anisotropy in tibia bone requires defining the orientation of major anisotropy axes, which is not necessarily the same throughout the tibia. For example, the trabecular bone in the epiphysis may have different anisotropy axis than the diaphyseal cortical bone. This highlights the difficulty of accurately defining the major anisotropy axes in trabecular bone. Ün et al. pointed out that the literature still lacks a realistic mechanical analysis of bone that correctly accounts for its anisotropy and heterogeneity. At this time, there is still no consensus on the choice of anisotropic power-law that could finally propose significantly superior anisotropic model than the isotropic approach [Ün2016]. Recently, anisotropic power laws were identified for trabecular bone of the proximal tibia by Munford et al. in 2020 [Munford2020]. In the future, we expect that reliable standard methods fully characterize bone anisotropy as a function of density. Numerical models of bone based on tomography and segmentation will be able to provide more accurate simulations of the mechanical behavior of bone.

In our study, we did not focus on local bone strength or damage accumulation. Instead, we only on force transmission from the proximal and distal parts of the tibia on the biomaterial implanted in the bone defect. Moreover, we only considered axial compression of the tibia and were only interested in loading a diaphyseal biomaterial. The axial components of stress and strains in the diaphyseal biomaterial are the same whether the material assignment is isotropic or anisotropic, with the Young's modulus values in the longitudinal direction being the same in both formulations. We therefore considered that the isotropic elastic model used in this study was simpler and more appropriate choice, compared to a more complex anisotropic model, whose axes of anisotropic could not be defined rigorously.

4.6 Accuracy of finite element model mesh

The quality of the tibia and biomaterial meshes was validated by an Abaqus mesh verification analysis keeping the standard threshold values proposed by default (Table 1). The mesh of the biomaterial is fully structured and homogeneous; it does not contain any defect. The mesh of the tibia is homogeneous on the surface but heterogeneous within. We have also checked mesh analysis with strict threshold values that should be used in a biomechanical finite element calculation as recommend by Burkhart et al. in 2013 [Burkhart2013]. According to the latter criteria, the mesh of the tibia is 91% accurate (Table 1), which is a very acceptable level following recommendation from Burkart et al. 2013.

4.7 Limits of the study

As limits of our study, we can argue that the tibia specimen we modelled is from elderly individual and may be significantly weaker in terms of mechanical properties and biological activity than the bone of younger individual who could to benefit from the implantation of a biomaterial.

We should add that our study only addressed the influence of mechanical loading on tissue differentiation in the diaphyseal defect based on Prendergast's model of mechanoregulation. The tissue differentiation results we obtained within the porous biomaterial are based on its complete colonization by cells from the very start of the simulation. We did not consider the process of cell invasion, neither due to cell migration nor proliferation. This prevents us from discussing the influence of this process which is often a problem in tissue engineering, as cells often remain at the periphery of the scaffold. Although our scaffold is shaped as a porous and hollow tube to promote cell invasion both from the internal and external boundaries, it is still possible that in reality less tissue is formed with in the thickness of the scaffold due to limited cell colonization.

4.8 Application of in silico results to dynamic fixators

The literature clearly establishes that the correction of a large diaphyseal bone defect in long bone depends primarily on its stabilization [Perren1977]. However, clinical and pre-clinical studies based on flexible fixators showed that limited inter-fragmental strains may accelerate bone healing [Augat2021]. Dynamic orthopedic systems with controlled flexibility have been developed to allow limited mechanical strain on the healing zone. These innovative systems are dynamic external fixators [Borgiani2019] or dynamic intramedullary nails [Dailey2021]. Plates locked with distal cortical screws or dynamic screws can also be a dynamic osteosynthesis device [Richter 2015, Bottlang2010, Boerckel2012]. Such dynamic devices could be used to treat the study case we considered, a 60-mm-wide diaphyseal bone defect filled with a porous biomaterial. In this case, the dynamic device loading should target the 0.1 mm level of distal displacement that we identified in silico as the best mechanical stimulation that led to mature bone formation.

5. Conclusion

By implementing Prendergast's and Lacroix's mechano-regulation model in a large defect in diaphyseal bone of the tibia, we identified the best mechanical stimuli for optimal bone healing. We considered that the bone defect was filled by a hollow porous PLA scaffold wrapped by a hydrogel membrane mimicking the periosteum. The results of our simulations verify our initial hypothesis. The mechanical quality of the bone tissue formed depends on local mechanical stresses. This in silico modeling approach allowed us to compare different mechanical load conditions based on the imposed relative displacement of both bone extremities. We, therefore, selected the solution that favored the formation mature bone. Ultimately, the strategy to be adopted and the clinical response must involve

the clinicians, the rehabilitation workers and the experts in biomechanics to optimize and integrate patient-dependent specificities. This study, thus offers a new perspective and could be part of an overall approach to better promote bone repair and faster recovery.

6. Acknowledgements

The authors declare no conflict of interest.

6. Ethics approval and consent to participate

Local ethics committee approval was not required to use a scan from an anonymized cadaveric sample. The protocol of this study was approved by the scientific committee of our anatomical department.

7. References

[Anderson1967]. Anderson CB. Mechanics of fluids. In: Baumeister T (ed) Marks' saturated handbook of mechanical engineers, 1967. pp 3.48–3.76

[Augat2021] Augat P, Hollensteiner M, von Rüden C. The role of mechanical stimulation in the enhancement of bone healing. Injury 52S2 (2021) S78–S83. https://doi.org/10.1016/j.injury.2020.10.009

[Boccaccio2008] A. Boccaccio, P. Prendergast, C. Pappalettere, et al. 2008. Tissue differentiation and bone regeneration in an osteotomized mandible: a computational analysis of the latency period. Med Biol Eng Comput 46: 283–298.

[Boerckel2012] Joel D. Boerckel, Yash M. Kolambkar, Hazel Y. Stevens, Angela S.P. Lin, Kenneth M. Dupont, and Robert E. Guldberg. Effects of in vivo mechanical loading on large bone defect regeneration. J Orthop Res. 2012 July ; 30(7): 1067–1075. doi:10.1002/jor.22042.

[Bottlang2010] Bottlang M, Lesser M, Koerber J, et al. Far cortical locking can improve healing of fractures stabilized with locking plates. J Bone Joint Surg Am. 2010;92(7):1652-1660. doi:10.2106/JBJS.I.01111

[Burkhart2013] Burkhart TA, Andrews DM, Dunning CE. 2013. Finite element modeling mesh quality, energy balance and validation methods: a review with recommendations associated with the modeling of bone tissue. J Biomech. 46(9):1477–1488.

519 [Casanova2010] R. Casanova, D. Moukoko, M. Pithioux, C. Pailler-Mattéi, H. Zahouani, P. Chabrand.
520 Temporal evolution of skeletal regenerated tissue: what can mechanical investigation add to
521 biological?, Med. and Biol. Eng. & Comp., 2010, 48(8):811-819.

522 [Checa2010] S. Checa D. P. Byrne J. Pendergast: Predictive modeling in mechanobiology : combining
523 algorithms for cell activites in response to physical stimuli using lattice-modelling approach. Computer
524 methods in mechanics, ASM 1, 2010, pp. 423-435

525 [Claes1997] Claes L, Augat P, Suger G, Wilke HJ. Influence of Size and Stability of the Osteotomy Gap
526 on the Success of Fracture Healing. Journal of Orthopaedic Research 1997, 15:577-584

527 [Coïc2010]. M. Coïc, V. Placet, E. Jacquet, C. Meyer. Mechanical properties of collagen membranes
528 used in guided bone regeneration: a comparative study of three models. Rev Stomatol Chir Maxillofac.
529 2010 ;111(5-6):286-90. doi: 10.1016/j.stomax.2010.10.006.

530 [Dailey2021] Dailey HL, Schwarzenberg P, Webb Iii EB, Boran SAM, Guerin S, Harty JA. Pilot study of
531 micromotion nailing for mechanical stimulation of tibial fracture healing. Bone Jt Open.
532 2021;2(10):825-833. doi:10.1302/2633-1462.210.BJO-2021-0121.R1

533 [Gardner1997] Gardner TN, Evans M, Hardy J, Kenwright J. Dynamic interfragmentary motion in
534 fractures during routine patient activity. Clin Orthop Relat Res 1997(336):216–25.

535 [Hamandi2022] Hamandi, F.; Tsatalis, J.T.; Goswami, T. Retrospective Evaluation and Framework
536 Development of Bone Anisotropic Material Behavior Compared with Elastic, Elastic-Plastic, and Hyper-
537 Elastic Properties. Bioengineering 2022, 9, 9. https://doi.org/10.3390/bioengineering9010009”

538 [Harris2008] M. Charles-Harris M. A. Koch M. Navarro D. Lacroix E. Engel· J. A. Planell : A PLA/calcium
539 phosphate degradable composite material for bone tissue engineering : an vitro study. Mater Med,
540 2008,19:1503-1513.

541 [Hobatho1997] M.C. Hobatho, J.Y. Rho, R.B. Ashman. Anatomical Variation of Human Cancellous Bone
542 Mechanical Properties In Vitro. Studies in Health Technology and Informatics, 1997, Vol. 40, 157-173

543 [Hwang2010] C.M. Hwang, S. Sant, M. Masaeli, et al. Fabrication of three-dimensional porous cell-
544 laden hydrogel for tissue engineering. Biofabrication. 2010;2(3):035003.

545 [Isaksson2006] Isaksson H, Donkelaar CCv, Huiskes R, et al. 2006. Corroboration of mechanoregulatory
546 algorithms for tissue differentiation during fracture healing: comparison with in vivo results. J
547 Orthopaed Res 24: 898– 907.

[Lacroix2002] D Lacroix P.J. Prendergast. A mechano-regulation model for tissue differentiation during fracture healing: analysis of gap size and loading. Journal of Biomechanics 2002, 35, 1163-1171.

[Masquelet2012] A.-C. Masquelet, J. Sales de Gauzy, T. Bauer, A. Fabre, F. Fitoussi, D. Hannouche, J.-L. Jouve, C. Karger, D. Le Nen, H. Mathevon, P. Merloz, L. Obert, A. Poichotte, S. Rigal, et la Société française de chirurgie orthopédique et traumatologique. Reconstruction of post-traumatic diaphyseal bone defects : Preoperative planning, guideline, and future developments. Revue de Chirurgie Orthopédique et Traumatologique, 2012, 98, 1, Pages94-103.

[Milan2010] J. L. Milan, J. A. Planell, D. Lacroix. Simulation of bone tissue formation within a porous scaffold under dynamic compression. Biomech Model Mechanobiol, 2010, 9:583-596

[Munford2020] Munford, M. J., Ng, K. C. G., Jeffers, J. R. T., Mapping the Multi-Directional Mechanical Properties of Bone in the Proximal Tibia. Adv. Funct. Mater. 2020, 30, 2004323. https://doi.org/10.1002/adfm.202004323

[Navarro2006] M. Navarro, C. Aparicio, M. Charles-Harris, M.P. Ginebra, E. Engel, J. A. Planell : Development of a biodegradable composite scaffold for bone tissue engineering: Physicochemical, Topographical, Mechanical, Degradation, and Biological Properties. Adv Polym Sci, 2006, 200: 209-231

[Oliveira2010] S.M. Oliveira, R.A. Ringshia, R.Z. LeGeros, E. Clark, M.J. Yost, L. Terracio & C.C. Teixeira. An improved Collagen Scaffold for Skeletal Regeneration. Journal of Biomedical Materials Research. Part A, 2010, 94(2), 371–379. http://doi.org/10.1002/jbm.a.32694

[Palomares2010] K. T. S. Palomares, R.E. Gleason, Z.D. Mason, D.M. Cullinane, T.A. Einhorn, L.C. Gerstenfeld, & E.F. Morgan. Mechanical stimulation alters tissue differentiation and molecular expression during bone healing. Journal of Orthopaedic Research : Official Publication of the Orthopaedic Research Society, 2009, 27(9), 1123–1132. http://doi.org/10.1002/jor.20863

[Peng2006] L. Peng, J. Bai, X. Zeng, Y. Zhou. Comparison of isotropic and orthotropic material property assignments on femoral finite element models under two loading conditions. Med Eng Phys, 28 (2006), pp. 227-233

[Perier-Metz2020] Perier-Metz C, Duda GN and Checa S (2020) Mechano-Biological Computer Model of Scaffold-Supported Bone Regeneration: Effect of Bone Graft and Scaffold Structure on Large Bone Defect Tissue Patterning. Front. Bioeng. Biotechnol. 8:585799. doi: 10.3389/fbioe.2020.585799

[Perren1977] Perren SM, Cordey J. [Tissue differences in fracture healing (author's transl)]. Unfallheilkunde 1977;80(5):161–4.

[Perren2015] Perren SM. Fracture healing: fracture healing understood as the result of a fascinating cascade of physical and biological interactions. Part II. Acta Chir Orthop Traumatol Cech. 2015;82(1):13–21

[Pobloth2018]. Pobloth AM, Checa S, Razi H, et al. Mechanobiologically optimized 3D titanium-mesh scaffolds enhance bone regeneration in critical segmental defects in sheep. Science Translational Medicine. 2018 Jan;10(423). DOI: 10.1126/scitranslmed.aam8828. PMID: 29321260

[Prendergast1997] Prendergast PJ, Huiskes R, Soballe K (1997) Biophysical stimuli on cells during tissue differentiation at implant interfaces. J Biomech 30:539–548

[Richter2015] Richter, Henning; Plecko, Michael; Andermatt, Daniel; Frigg, Robert; Kronen, Peter W; Klein, Karina; Nuss, Katja M; Ferguson, Stephen J; Stöckle, Ulrich; von Rechenberg, Brigitte (2015). Dynamization at the near cortex in locking plate osteosynthesis by means of dynamic locking screws: an experimental study of transverse tibial osteotomies in sheep. Journal Bone Joint Surgery America, 97(3):208-215.

[Rolland1995] E. Rolland, G. Saillant: La consolidation osseuse normale et pathologique. Ann Réadaption Med Phys, 1995, 38, 245-251

[Sandino2010] C. Sandino S. Checa, P. J. Prendergast, D. Lacroix.: Simulation of angiogenesis and cell differentiation in a CaP scaffold subjected to compressive strains using a lattice modeling approach. C. Sandino S. Checa, P. J. Prendergast, D. Lacroix. Biomaterials Volume 31, Issue 8, March 2010, Pages 2446–2452

[Sheikh2015] Z. Sheikh, S. Najeeb, Z. Khurshid, V. Verma, H. Rashid, M. Glogauer. Biodegradable Materials for Bone Repair and Tissue Engineering Applications. Materials 2015, 8, 5744-5794; doi:10.3390/ma8095273.

[Snyder1991] S. M. Snyder, E. Schneider. Estimation of mechanical properties of cortical bone by computed tomography. 1991. Journal of Orthopaedic Research, 3, 1991, Pages 422-431, https://doi.org/10.1002/jor.11000903159

[Taddei2006] Fulvia Taddei, Luca Cristofolini, Saulo Martelli, H.S. Gill, Marco Viceconti, Subject-specific finite element models of long bones: An in vitro evaluation of the overall accuracy, Journal of Biomechanics, Volume 39, Issue 13, 2006, Pages 2457-2467, https://doi.org/10.1016/j.jbiomech.2005.07.018.

[Taylor2002] Taylor, W.; Roland, E.; Ploeg, H.-L.; Hertig, D.; Klabunde, R.; Warner, M.; Tho, M.-C.H.B.; Rakotomanana, L.; Clift, S. Determination of orthotropic bone elastic constants using FEA and modal analysis. J. Biomech. 2002, 35, 767–773.

[Ün2016]. Kerem Ün & Ahmet Çalık (2016) Relevance of inhomogeneous–anisotropic models of human cortical bone: a tibia study using the finite element method, Biotechnology & Biotechnological Equipment, 30:3, 538-547, DOI:10.1080/13102818.2016.1154803

[Victoria2009] G. Victoria, B. Petrisor, B. Drew & D. Dick. Bone stimulation for fracture healing: What's all the fuss? Indian Journal of Orthopaedics, 2009, 43(2), 117–120. http://doi.org/10.4103/0019-5413.50844

[Wang2016] J. Wang, L. Wang, Z. Zhou, H. Lai, P. Xu, L. Liao, J. Wei. Biodegradable Polymer Membranes Applied in Guided Bone/Tissue Regeneration: A Review. Polymers 2016, 8, 115; doi:10.3390/polym8040115

[Wirtz2000] Wirtz, D.C.; Schiffers, N.; Pandorf, T.; Radermacher, K.; Weichert, D.; Forst, R. Critical evaluation of known bone material properties to realize anisotropic FE-simulation of the proximal femur. J. Biomech. 2000, 33, 1325–1330.

[Yang2010] Haisheng Yang, Xin Ma, Tongtong Guo, Some factors that affect the comparison between isotropic and orthotropic inhomogeneous finite element material models of femur, Medical Engineering & Physics, Volume 32, Issue 6, 2010, Pages 553-560, ISSN 1350-4533, https://doi.org/10.1016/j.medengphy.2010.01.004.

[Yue2020] Yue S, He H, Li B, Hou T. Hydrogel as a Biomaterial for Bone Tissue Engineering: A Review. Nanomaterials (Basel). 2020 Jul 31;10(8):1511. doi: 10.3390/nano10081511. PMID: 32752105; PMCID: PMC7466535.

[Zhao2018] Zhao F, Mc Garrigle MJ, Vaughan TJ, McNamara LM. In silico study of bone tissue regeneration in an idealised porous hydrogel scaffold using a mechano-regulation algorithm. Biomech Model Mechanobiol. 2018 Feb;17(1):5-18. doi: 10.1007/s10237-017-0941-3